JOURNAL OF PROPULSION AND POWER
Vol. 9, No. 4, July–Aug. 1993

Diagnostics and Performance of a Low-Power MPD Thruster with Applied Magnetic Nozzle

T. M. York,* C. Zakrzwski,† and G. Soulas†
Ohio State University, Columbus, Ohio 43210

This study evaluates the performance of a 50–150-kW thruster which was ½-scale of a bench mark magnetoplasmadynamic (MPD) thruster; it was operated with and without applied magnetic nozzle fields. Capacitors (14 μF) and inductors (80 μH) in networks produced relatively constant currents for about 450 μs to generate the applied magnetic nozzle, and currents up to 2.3-kA constant for about 300 μs to drive the thruster. With the solid copper electrode, the applied magnetic field was excluded from the thrust chamber because of the short duration of the experiments. The ½-scale device was mass starved below $\dot{m}$ = 0.135 g/s; this was equivalent to 2 g/s for a full-scale MPD thruster with the same $\dot{m}/A$. With $\dot{m}$ > 0.25 g/s, the device was found to operate smoothly and with little evident erosion. Current-voltage records were similar with and without applied magnetic nozzle fields, indicating little effect of the external nozzles on the power deposition. The current plume in the expansion region outside the thruster chamber was reduced in axial extent with the application of the magnetic nozzle in this transient experiment. Momentum flux in the exhaust flow was measured by local pressure probes. For the same arc power, impact pressures with magnetic nozzles applied were 3–4 times larger than the self-field cases. Also, impact pressure increased with thruster power. For the 1.15- and 2.30-kA cases, thrust from integrated impact pressure increased by a factor of 1.6 with magnetic nozzles applied. Local electron density and temperature were determined using Langmuir probes; these values along with impact pressure were used to determine flow velocity. For the 1.15- and 2.30-kA cases, values of exhaust velocity increased by factors of 1.1 and 1.6, respectively, when the magnetic nozzles were applied.

Nomenclature

A_{cs} = cross-sectional area
B = magnetic induction
e = charge of electron
f = force per volume
I = discharge current
j = current density
k = Boltzman constant
l = length
m = particle mass
$\dot{m}$ = propellant mass flow rate
n = number density
Q = collision cross section
R = electrical resistance
r = radial dimension
$R_{A,C}$ = radius of anode, cathode
RC = resistance-capacitance time constant
Re_m = magnetic Reynolds number
T = temperature
T_{em} = electromagnetic thrust component
T_{eth} = electrothermal thrust component
U_{em} = electromagnetic velocity component
V = voltage
z = axial dimension
z_{ex} = axial length of the arc discharge electrodes
λ = coulomb collision parameter
λ_D = Debye length
λ_{in} = ion-neutral mean free path
μ = magnetic permeability
σ = conductivity

Subscripts
EMF = electromotive
e = electron
eff = effective
enc = enclosed
F = electrode fall
f = fully ionized
Ω = Ohm
TOT = total
w = weakly ionized

Introduction

ALTHOUGH a practical magnetoplasmadynamic (MPD) thruster has yet to be used for primary space propulsion, the MPD thruster may be the best realistic candidate to perform a variety of missions.[1,2] Proposed missions would require[2] an MPD thruster operating in the 10–100-kW power range with a specific impulse of 1000–3000 s. At such power levels the efficiency of self-field MPD thrusters, which rely solely on magnetic fields generated by the current through the propellant, is unacceptably low.[2] The use of an applied magnetic field which can act as a nozzle for the plasma flow may also serve to reduce frozen flow losses, and therefore, increase the efficiency of the thruster.[3–11] Presently, the physical processes that occur in the flow from a thruster with an applied magnetic field acting as a nozzle are not well understood.

A comprehensive review of MPD thruster performance was recently reported[1]; also, an overview of work performed on applied-field thrusters had been given by Seikel et al.[2] For devices operating in the 10–100-kW range, even at modest applied fields (0.1–0.15 T), thrust efficiencies were shown to improve. Studies of the effects of applied fields on the performance of megawatt-level pulsed thrusters were also re-

Presented as Paper 90-2665 at the AIAA/DGLR/JSASS 21st International Electric Propulsion Conference, Orlando, FL, July 18–20, 1990; received Jan. 28, 1991; revision received March 6, 1993; accepted for publication March 24, 1993.

*Professor, Aeronautical and Astronautical Engineering Department. Member AIAA.

†Graduate Research Associate, Aeronautical and Astronautical Engineering Department.

ported,[3] however, the acceleration processes in such devices were not understood. More extensive diagnostic studies were carried out on an applied-field pulsed megawatt MPD thruster experiment by Michels and York.[4,5] Results demonstrated that thrust and efficiency increased with applied fields. Derived values of thrust were observed to increase monotonically (B) with applied magnetic field strength.

Extensive diagnostic work was performed on a 25-kW applied-field lithium MPD thruster by Fradkin et al.[6] It was found that exit velocities approached 3×10^4 m/s, and thrust efficiencies approached 50%. A model proposed that the dominant acceleration contribution came from the conversion of rotational energy into directed energy by expansion in a magnetic nozzle.

In other work, Kimura and Yoshihiro[7] studied the reaction forces on a 300–1500 A MPD thruster and its surrounding magnetic nozzle coil; thrust stand measurements showed that thrust increased with magnetic field strength, which was varied up to 0.4 T. Tahara et al.[8] studied two versions of pulsed MPD thrusters which operated between 5–15 kA with various configurations of applied fields; field-related improvements included decreased discharge voltage, increased thrust, and decreased cathode erosion. Arakawa and Sasoh[9] studied a 10-kW power level thruster fitted with permanent magnets; electromagnetic forces related to the applied field contributed to a large percentage of the thrust. In an experimental study of significance to the present work, Kuriki and Okada[10] studied the effects of a magnetic nozzle arrangement on plasma generated by an 800-A arcjet. With $T_e = 4000$ K and $n_e = 5 \times 10^{13}$ cm^{-3}, the magnetic nozzle channeled the flow within the field lines and an electromagnetic force was involved in accelerating the weakly ionized plasma.

A more recent investigation of 100-kW class applied-field MPD thrusters was carried out by Mantenieks et al.[11] For all configurations tested, thrust increased with increased applied-field strength; for one configuration, the thrust increased by 64% when the magnetic field was increased to 0.3 T.

With the limited power available in space (100 kW), smaller size devices have the potential to be more efficient at low power levels.[12–14] Although various geometries (configurations)[12] have been evaluated, investigations of MPD thruster scaling have primarily considered pulsed thrusters operating in the megawatt range.[13,14] Gilland and Kelly[15] carried out a study of self-field MPD scaling using full- and $\frac{1}{2}$-scale versions of both the bench mark and flared anode thrusters. The full-scale devices were found to be more efficient for almost all power levels at equivalent specific impulses. In the light of such conflicting evidence, it is important to attempt to clarify the performance of arc and MPD arc devices of various sizes and power levels.

Apparatus

$\frac{1}{4}$-Scale MPD Thruster

A schematic of the $\frac{1}{4}$-scale MPD thruster is shown in Fig. 1. The thruster was constructed with a solid copper anode having an i.d. of 2.5 cm and an o.d. of 4.5 cm, and a solid 2% thoriated tungsten cathode having a diameter of 0.5 cm. The lengths of the anode and cathode were 1.25 cm, measured from the boron nitride backplate. This thruster was fashioned after the Air Force Aeronautics Laboratory (AFAL) $\frac{1}{2}$-scale variable-geometry MPD thruster, so that direct comparisons between the two devices could be made. The propellant studied was nitrogen, which allowed comparison with earlier work.[4,5] The boron nitride backplate had 15 holes drilled to serve as gas feed ports.

Propellant was injected by means of a specially designed gas feed system. The components of this system included a reserve gas plenum, the plenum in the thruster, and a high-speed electrical valve between the plena. The electrical valve (Skinner model VS20B2100), with $\frac{3}{8}$-in.-diam passage, was

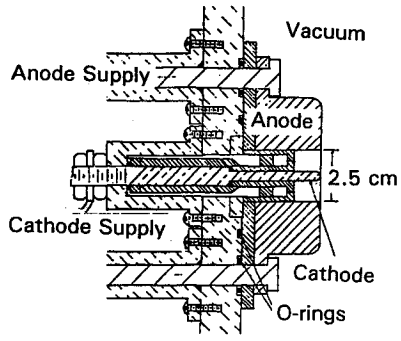

Fig. 1 Schematic of $\frac{1}{4}$-scale thruster.

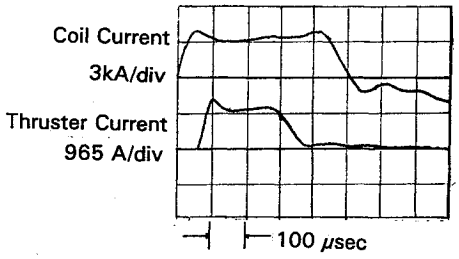

Fig. 2 Current waveforms for $\frac{1}{4}$-scale thruster and applied magnetic field coil.

overdriven to achieve fast opening. The pressure was seen to increase linearly for 5 ms, and then remain constant at the pressure of the reserve plenum. Mass flow rate determined from pressure probes in the chamber agreed with that determined from pressure drop in the reserve plenum.

The thruster pulse forming network (PFN) was designed to produce a 300-μs current pulse with amplitudes ranging from 0.7- to 2.3-kA constant for a quasisteady period of 200 μs. The magnetic nozzle system was designed to produce a 500-μs pulse for the solenoidal coil with currents between 1.3- and 2.7-kA constant for a quasisteady period of approximately 450 μs. The major components of each of the discharge systems included the PFN, switches for the PFN, a dc power supply capable of charging the PFN over a range of different voltages, and a timing system to control the firing sequence.

The PFN were separate inductance-capacitance (L-C) ladders operated independently. Typical current records are presented in Fig. 2; the thruster PFN was charged to 7 kV, and the magnetic field coil PFN to 13 kV. The thruster current was delayed 70 μs from the start of the magnetic field current; this delay allowed the magnetic field to establish itself before the steady-state portion of the thruster current occurred.

The main components of the vacuum system included 6-in.-diam "cross" and "T" shape Pyrex® ducts, a vacuum pump, gate valves, and vacuum gauges. These components were assembled to provide the optimum arrangement for thruster, magnetic field coil, and the performance of diagnostic studies. The thruster was mounted on one arm of the cross, with the coil encircling the vacuum vessel. The base pressure achieved in this system was less than 1 mTorr; the total volume enclosed above the gate valve was 0.0304 m^3.

Diagnostics Devices

Two Rogowski loops were used to monitor circuit currents; calibrations (with integrator time constant = 8.84 ms) were carried out with ringing L-C discharges. A 1000:1 voltage probe (P6105 High Voltage Probe, Tektronix, Portland, Oregon) was used.

Axial magnetic field probes and several probes that measured radial/azimuthal magnetic fields were fabricated from multiturn loops placed in a 6-mm o.d. Pyrex tube with a sealed

end. The axial probe had 50 turns in 14-mm length; the radial/azimuthal probe had 140 turns in 3-mm length. An active integrator[16] was used. Calibration was carried out with a single-turn solenoid driven by an L-C discharge.

A pressure probe was used in this study to measure the impact pressure in the expansion region of the ¼-scale MPD thruster; it utilized a piezoelectric transducer enclosed in a 1-cm-diam quartz tube, sealed squarely at the end.[4] The system included a battery powered 10× amplifier and follower unit. A 1-cm-long, 1-cm-diam Pyrex isolator was attached to the sensing end of the quartz tube; it eliminated initial stress waves and acted as a thermal insulator. Probes were calibrated in a shock tube.

A double langmuir probe was used to determine electron temperature and number density in the exhaust. The probe electrodes were 0.127-mm-diam tungsten wire, 1-cm long and separated by a distance of 5 mm. The voltage bias across the probe elements was supplied by a variable charge 500-μF capacitor. The probe current was monitored with a Tektronix P6021 current probe.

Operating Conditions—Scaling Considerations

The variation of the size of thrusters is fundamental to the scaling process. Values for the sizes of thrusters of interest here are shown in Table 1.

The mass flow rate was scaled so that the mass flux ($\dot{m}/A_{cs}$) of gas in the discharge chamber remained a constant; accordingly, the ¼-scale thruster mass flow rate was defined as $\frac{1}{16}$ the full-scale value (Table 1). Mass starvation effects were evident, and an acceptable mass flow rate for this device was determined by experiment to be 0.135 g/s.

Since the applied field did not penetrate the discharge chamber, the scaling of the ¼-size thruster will be treated as a self-field device. Some parameters considered when scaling thrusters are given in Table 1. While U_{em} has been used to scale thrusters, this study attempted to scale based on plasma interactions being locally equivalent to full scale: $\vec{j} \times \vec{B}$ and $\dot{m}/A_{cs}$ were maintained. For the electromagnetic thrust mechanism the force density can be expressed as

$$\vec{f} = \vec{j} \times \vec{B} \propto [I^2/(r^2 \cdot z)]\alpha j^2 z \tag{1}$$

With the geometry being scaled by ¼, and the specification that $\vec{j} \times \vec{B}$ be maintained from the full- to ¼-scale, the ¼-scale thruster should then be operated at currents which are ⅛ of those in full-scale thrusters. For this study, the ¼-scale thruster was operated at two current levels, 1.15 and 2.3 kA, which correspond to full-scale currents of 9.2 and 18.4 kA, respectively.

The velocity associated with the electromagnetic-thrust component can be expressed as

$$U_{em} = \frac{T_{em}}{\dot{m}} = \left(\frac{I^2}{\dot{m}}\right)\frac{\mu_0}{4\pi}\ell_n\left(\frac{R_A}{R_C}\right) \tag{2}$$

So

$$U_{em} \propto \frac{I^2}{\dot{m}} \propto \frac{j^2}{(\dot{m}/A_{cs})} \cdot z^2 \propto \frac{jB}{(\dot{m}/A_{cs})} z$$

If $\vec{j} \times \vec{B}$ and $\dot{m}/A_{cs}$ were maintained, then I (scaled) would be decreased; $U_{em} \propto z$, and so would decrease with size, in this case by a factor of ¼.

For the electrothermal thrust component, velocity scaling depends on the plasma conductivity. The input power is determined by I^2R; this is proportional to the kinetic power of the exhaust, $\dot{m}u_e^2/2$. Therefore, taking $\vec{j} \times \vec{B}$ and $\dot{m}/A_{cs}$ as fixed, if the resistance across the electrodes were a constant for different devices (i.e., if sheath drops were dominant) the electrothermal velocity component would scale with $z^{1/2}$. If the conductivity of the plasma were constant and plasma voltage drops were dominant, the electrothermal velocity would be a constant for different devices.

Typical geometry and current values for the bench mark[14] full-scale thruster and for the AFAL[15] ½-scale thruster are shown in Table 1 for comparison. Since I^2 is proportional to self-field thrust, $I^2/\dot{m}$ is proportional to the specific impulse for the self-field MPD thruster, assuming that the electromagnetic thrust component is dominant. Operation of the ¼-scale thruster at 2.3 kA produces $I^2/\dot{m}$ = 39 kA²s/g, a value appropriate for comparison with a range of thrusters.

Applied Magnetic Nozzle Fields

The applied magnetic field geometry used to guide the plasma was generated by a solenoidal coil designed to produce magnetic field lines that diverged in a reasonable manner. The magnetic coil was constructed with five layers of ¼-in.-diam solid copper wire wrapped around an 8.75-in.-o.d. PVC pipe.

Table 1 Thruster scaling parameters

Size[a]					
Scale	Cathode radius, cm	Anode radius, cm	Anode length, cm	Cathode depth, cm	R_A/R_C
¼ (OSU)	0.25	1.25	1.25	1.25	5.0
½ (AFAL)	0.50	2.50	Variable	Variable	5.0
Full (Princeton)	0.90	5.00	10.00	5.00	5.6
Mass flow rate[b]; electromagnetic acceleration force density[c]					
	I, kA	R_A, cm	Z_{ex}, cm	$j \times B_0$, kN/m³	
¼-Scale	1.25	1.25	1.25	25.46	
Full-scale	10.0	5.0	5.0	25.46	
Electromagnetic velocity component[d]					
	$\dot{m}$, g/s	I, kA	$I^2/\dot{m}$, kA²·s/g	U_{em}, m/s	
Princeton-full scale	2.0	18.4	157	23,500	
	2.0	10.0	46	6,900	
OSU-¼ Scale	0.14	2.3	39	5,900	
	0.14	5.0	85	12,700	

[a]Principle: preserve length proportions. [b]Principle: preserve $\dot{m}/A_{cs}$; $\dot{m}_{(1/4\text{-scale})} = (\frac{1}{16})\dot{m}_{(\text{full-scale})}$. [c]Principle: preserve force per unit volume. [d]Principle: preserve $U_{em} = T_{em}/\dot{m}$.

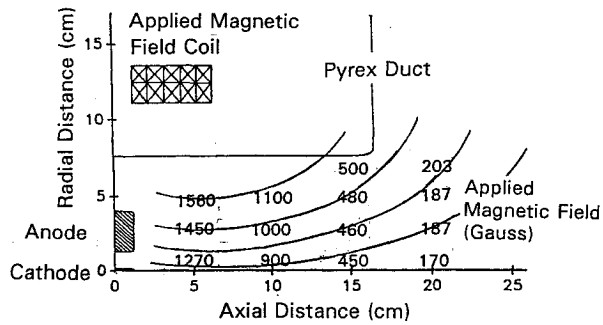

Fig. 3 Thruster, field coil, and vacuum vessel schematic with applied magnetic field lines (local values, in Gauss).

Current of 2.8 kA produced a maximum magnetic field strength of 1.27 kG along the axis of the coil when the ¼-scale thruster was in place.

The applied magnetic field strength distribution was mapped from measurements with radial and axial magnetic field probes. A sketch of the magnetic flux lines with respect to the position of the thruster is shown in Fig. 3; the throat, or minimum area, of the magnetic flux lines occurred at approximately 2.5 cm from the face of the thruster on the axis of the coil. The magnetic field distribution was influenced by the field exclusion from the solid copper anode during the time period of the experiment.

The magnitude of the magnetic field was appropriate for the confinement of the plasma with kinetic pressure (nkT = 3×10^3 N/m^2 for $n_e = 10^{16}$ cm^3, $T_e = 2$ eV) exceeded by magnetic pressure ($B^2/8\pi = 4 \times 10^3$ N/m^2 for $B = 1$ kG).

One-Fourth Scale Thruster Experimental Data

Propellent Mass Flow Rate

The lower limit on $\dot{m}$ was determined using several diagnostics. Current-voltage characteristics for the thruster were first recorded for a mass flow rate of 0.034 g/s of nitrogen; this corresponded to 0.5 g/s full-scale. The voltage records indicated that the thruster was operating in an erratic fashion, with evident high-frequency oscillations. When the mass flow rate was increased to 0.068 g/s, the oscillations were significantly reduced, but occasionally there were still high-frequency oscillations at 1.15 kA. Local B_θ magnetic field probes in the exhaust plume showed large oscillations in the magnetic field during the steady-state portion of the thruster current history. The oscillations varied from shot-to-shot; they were typical of an unstable arc that may have been rotating.

It was concluded that the cathode was mass-starved because of an uneven distribution of gas in the discharge chamber; eight ports were located radially midway between the electrodes. To overcome this problem, seven gas ports (0.36-mm in diameter) were added around the base of the cathode, approximately 1.5 mm from the cathode radius. In the new injection configuration, a mass flow rate of 0.135 g/s was the lowest rate that produced smooth and predictable magnetic field records; these were taken as an indication of smooth discharge operation. All of the test results presented in this study used a mass flow rate of 0.135 g/s; this corresponds to a mass flow rate of 2.16 g/s for a full-scale thruster.

The background pressure for the ¼-scale MPD thruster was higher from beginning to end of the thrust period (1–7 mTorr) than those of bench mark[14] (0.1–4.0 mTorr), AFAL ½ (0.1–3.5 mTorr) devices; however, evidence has suggested that background pressures of 10 mTorr or less have a minor effect on thrust and voltage measurements for steady-state self-field thrusters.

Current-Voltage Characteristics

Arc currents over the range of 0.86–2.3 kA were obtained by varying the thruster PFN voltage over the range of 5–13 kV. Anode-cathode voltage drops and discharge currents were measured for intervals of 0.5 kV on the thruster PFN.

The applied-field and self-field data are shown, with error bars, in Fig. 4. Each point represents data taken at a fixed time, 200 μs from the start of thruster current, for a large number (4–5) discharges of the thruster. Data were taken in intervals of 0.5 kV on the thruster PFN, going from low- to high-charge voltage and reversing the sequence; this was then repeated.

Local Magnetic Field Measurements

The current distribution in the electrical discharge of the ¼-scale MPD thruster was mapped from local azimuthal magnetic field measurements for thruster currents of 1.15 and 2.3 kA for both applied-field and self-field cases. Data were taken at radial positions varying from 0.6 to 2.5 cm, and at axial positions ranging from 0.3 to 25 cm from the backplate of the thruster.

The azimuthal magnetic field measurements were used to calculate the current enclosed within a given radius at a given axial position as

$$I_{enc}(r, z) = [2\pi r B(r, z)/\mu_0] \quad (3)$$

A sketch of current profiles for self-field and applied-field cases is shown in Fig. 5; the dashed lines are extrapolations.

Impact Pressure Profiles

Radial profiles of impact pressure in the exhaust plume of the ¼-scale thruster were recorded for axial locations 5, 9, 14, and 20 cm from the face of the thruster. The pressure profiles were measured for 1.15- and 2.3-kA currents, and for both applied-field and self-field cases. The radial profiles for the 1.15-kA level are shown in Figs. 6 and 7. The pressure reported for each position is a value taken in the relatively constant current portion of individual pressure records after initial transients had terminated. The impact pressure data indicate that the exhaust plume was symmetrical about the

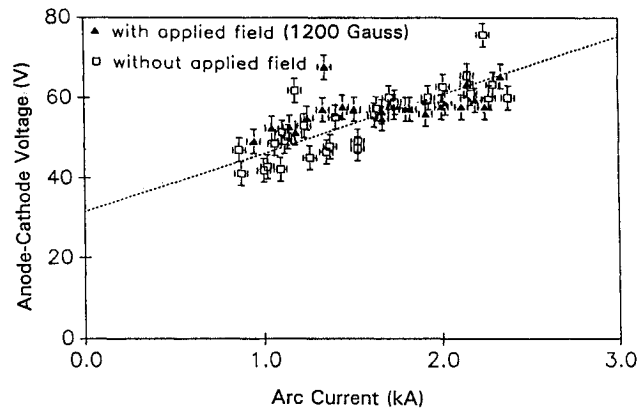

Fig. 4 Current-voltage characteristics of ¼-scale MPD arc thruster.

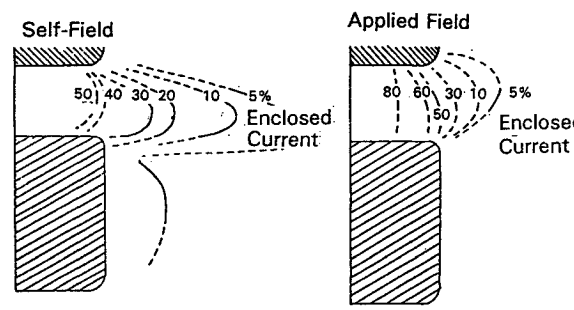

Fig. 5 Enclosed current contours without and with applied field with arc current, I = 2.3 kA and $\dot{m}$ = 0.135 g/s.

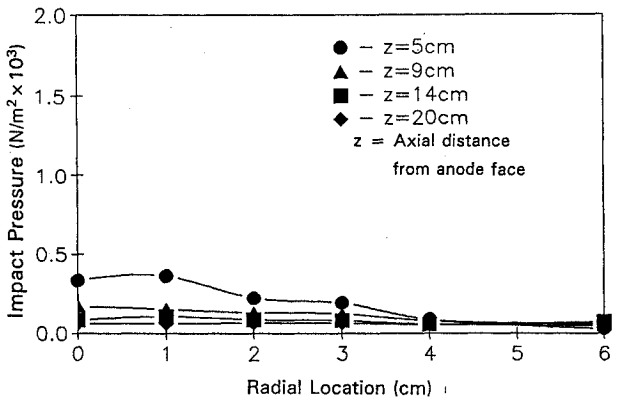

Fig. 6 Impact pressure radial profile with arc current, I = 1.15 kA, self-field.

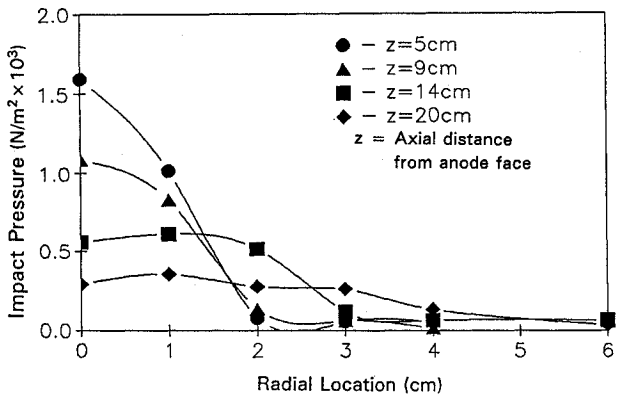

Fig. 7 Impact pressure radial profile with arc current, I = 1.15 kA, 1200 G applied field.

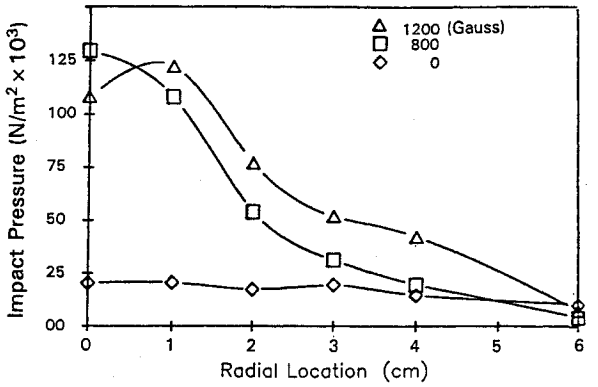

Fig. 8 Impact pressure radial profiles for self-field, 800-, and 1200-G applied fields (Z = 14 cm, I = 2.3 kA, $\dot{m}$ = 0.135 g/s).

axis and reproducible from shot-to-shot. Impact pressure data were also taken for a value of the applied magnetic field intermediate between 0 (self-field) and 1200 G. With a nominal value of 800 G at the center of the coil, impact pressure was measured at z = 14 cm with the thruster operating at 2.3 kA; pressure profiles for the 0, 800, and 1200 G cases are shown in Fig. 8.

Analysis and Interpretation of Data

Current-Voltage Measurements for the ¼-Scale Thruster

The data points recorded with and without the applied nozzle followed similar trends (Fig. 5), with scatter typical of I-V data for these types of measurements. The I-V variation can be best described as linear over the range of currents studied; this indicates dominance of the electrothermal thrust component. The linear relationship for the applied-field case was found to differ only slightly from that for the self-field case, for lower (<2.0 kA) currents. At higher currents, the applied magnetic field resulted in a slight decrease in arc voltage, but this variation was within the error bars and so will not be considered quantitatively. The thruster power was determined from I-V, and the two operating conditions:

$$P_{\mathrm{TOT}}(1.15\ \mathrm{kA}) = 53\ \mathrm{kW}$$

$$P_{\mathrm{TOT}}(2.3\ \mathrm{kA}) = 151\ \mathrm{kW}$$

For a given current, the deposition of power can be understood from components of the total voltage across the electrodes:

$$V_{\mathrm{TOT}} = V_{\Omega} + V_{\mathrm{EMF}} + V_F \qquad (4)$$

$$V_{\mathrm{TOT}} = \int j/\sigma\, \mathrm{d}l + \int (V \times B)\, \mathrm{d}l + V_F$$

The first term expresses the voltage drop due to the Ohmic resistance of the plasma. The second term is back-emf arising from the motion of the plasma normal to a magnetic field. The third term, V_F, is the electrode fall voltage; it includes electrode heating and plasma sheath losses. Losses due to dissociation and ionization are included in the Ohmic term and the fall voltage term. The fall voltage was determined by extrapolation of the voltage data to zero current (32.7 V). At the 1.15-kA level, the back-emf contributed 3 V, and at the 2.3-kA level it contributed 16.5 V. These estimates were made using a model for azimuthal magnetic field appropriate for MPD thruster blowing[19] and velocity values obtained from pressure measurements that will be described below.

Using the above evaluations, plasma temperatures can be estimated from the electrical conductivity of the plasma which was determined from the voltage measurements. Equation (4) can be rewritten

$$\sigma = (V_{\mathrm{TOT}} - V_{\mathrm{EMF}} - V_F)^{-1} \int J/(2\pi r z_0)\, \mathrm{d}r \qquad (5)$$

Uniform current density is assumed along the electrode length, z_0, and σ is assumed to be constant; the electrical conductivities are then

$$\sigma(1.15\ \mathrm{kA}) = 1900\ (\Omega\mathrm{m})^{-1}$$

$$\sigma(2.3\ \mathrm{kA}) = 2800\ (\Omega\mathrm{m})^{-1}$$

An approximate relationship for conductivity was first given by Spitzer for fully ionized plasmas[20]

$$\sigma_f = T_e^{3/2}/(5.2 \times 10^{-5}\, \ell n\, \lambda) \qquad (6)$$

where $\ell n\, \lambda$ typically has a value of 10 for a wide range of plasma densities and temperatures, and T_e is given in eV. In a weakly ionized plasma, electron-neutral collisions dominate; in that case we have[21]

$$\sigma_w = 0.532[e^2/(m_e k T_e)^{0.5}][n_e/(n_a Q)] \qquad (7)$$

where n_e is the electron density, n_a is the neutral atom density, and Q is the electron-neutral atom collision cross section. Accordingly, for a plasma with an arbitrary degree of ionization the electrical conductivity can be approximated by[21]

$$\sigma = (1/\sigma_f + 1/\sigma_w)^{-1} \qquad (8)$$

Using the above equations the electron temperatures are

$$T_e(1.15\ \mathrm{kA})\text{: } 1.0\ \mathrm{eV}$$

$$T_e(2.3\ \mathrm{kA})\text{: } 1.3\ \mathrm{eV}$$

Under the plasma conditions (n_e, T_e) in the experiment, the electron-ion equilibration time is about 3 μs, so $T_e = T_i$ is a reasonable assumption.

Current Distribution in the Exhaust Flow

For the self-field case (Fig. 5) as much as 40% of the current was blown past the end of the discharge chamber, typical for self-field MPD thrusters[14] with $Re_m \approx 10$. It has been shown to be desirable to have the current spread as far downstream as possible, because this enhances the electromagnetic thrust component.[22] However, the transient applied magnetic nozzle fields were found to restrict the discharge to a region closer to the chamber (Fig. 5). For the self-field case, 10% of the current was carried downstream a distance $2\frac{1}{2}$ times the anode radius from the backplate. In contrast, for the applied-field case, 10% of the current was carried downstream a distance only $1\frac{1}{2}$ times the anode radius from the backplate. For both cases, however, the same percentage of current moved past the arc chamber exit plane. With the langmuir probe indicated $\times 2$ increase of temperature with applied nozzle, the Re_m would have increased $\times 3$, which should enhance blowing effects. However, from the mapping of the magnetic flux lines and the tabulated values of magnetic field strengths, it is seen that the thruster exit plane lies in a region of converging magnetic field. It is probable that the magnetic field affected the confinement of the plasma carrying the current, holding it further upstream and channeling it along the axis through the magnetic nozzle in this transient discharge. The position $z = 2$ cm was the axial location nearest the thruster exit at which impact pressure was measured. For the self-field case $z = 2$ cm and $r = 1$ cm, the impact pressure was 3.9×10^3 N/m^2, while the calculated magnetic pressure at this point was 3.7×10^3 N/m^2.

Impact Pressure Measurements

From the impact pressure data, it is concluded that the applied magnetic nozzle fields significantly affected the plasma; the magnitude of the impact pressure increased within a 3-cm radius of the centerline for all axial positions. The magnitude of the discharge current also affected impact pressure, although 1.15- and 2.3-kA thruster currents exhibited similar radial profiles. The self-field pressure profiles for 1.15 kA (Fig. 6) have peak values of 100–400 Nm^{-2}, with e^{-1} radii of about 3 cm. Impact pressure decreased in magnitude downstream. The applied field pressure profiles are significantly different. For both 1.15- and 2.3-kA current levels a Gaussian-shaped profile was evident at the $z = 5$- and 9-cm locations, with the majority of the momentum flux being confined within a 2-cm radius. For the 1.15-kA level, peak pressures were 1500 Nm^{-2} and e^{-1} radius was about 1 cm, while for the 2.3-kA level the peak pressure was 3800 Nm^{-2} and e^{-1} radius was about 2 cm. At the $z = 14$-cm position the momentum flux for 1.15 kA was confined within the 3-cm radius, but for the 2.3-kA level, significant momentum flux occurred out to 5-cm radius. At the 20-cm location, both the 1.15- and 2.3-kA applied-field cases demonstrated broad, flat radial profiles.

The above data demonstrate that the applied magnetic nozzle fields generated impact pressures that were significantly higher than those for the self-field discharges at the same power level; the fields confined the plasma flow to smaller radii and allowed more gradual expansion. This is consistent with a degree of balance between the pressure from the applied magnetic field and the internal kinetic pressure of the plasma. Earlier reported experimental results[23] had shown that for a plasma in magnetic nozzle configurations, the plasma expansion was controlled by the magnetic pressure and was not controlled primarily by the shape of the magnetic field lines.

Langmuir Probe Measurements

The current-voltage characteristics of the cylindrical double langmuir probe were reduced to provide values of local electron temperature and electron number density. Analysis of the data included evaluation of the effects of low density (enhanced Debye collection), collisions, and magnetic field[24] on the particle collection. The size of the probe ($r = 6.35 \times 10^{-5}$ m) was on the order of the mean free paths ($\lambda_{ei} = 5 \times 10^{-5}$ m, $\lambda_{in} = 5 \times 10^{-5}$ m) and Debye length ($\lambda_d = 10^{-6}$–10^{-7} m). Collision effects proved to be minimal, but corrections for the enhanced collection due to thick sheaths were necessary; the approximate method of Kiel[24] was used. Regarding applied magnetic field effects, ion and electron Larmor radii were large enough to allow the weak B-field approximation[24] to be made.

Radial variations of electron density and temperature generally reinforce the conclusion from impact pressure data, i.e., less uniform and more highly peaked distributions with the applied field nozzles. Specifically, for the self-field discharges the plasma was ejected with relatively uniform temperature; neither T_e or N_e was strongly focused on axis.

Axial variations of T_e and N_e (Figs. 9 and 10) show that, generally, both were higher for the applied-field cases than for the self-field cases. As with the impact pressure data, values of T_e and N_e with applied-field were much larger near the axis. As power input was the same without and with applied field nozzles, it can be concluded that compression effects were significant within the magnetic nozzle fields. These effects of magnetic nozzles are similar to those reported by Kuriki and Okada,[10] who examined flow from a lower current (800 A) arcjet in a much larger vacuum vessel and with a large gap between the arc plasma source and the nozzle fields.

Temperatures for the self-field cases determined from local langmuir probes are in reasonable agreement with the temperatures estimated from conductivity. With the magnetic nozzle fields applied, however, there was a temperature enhance-

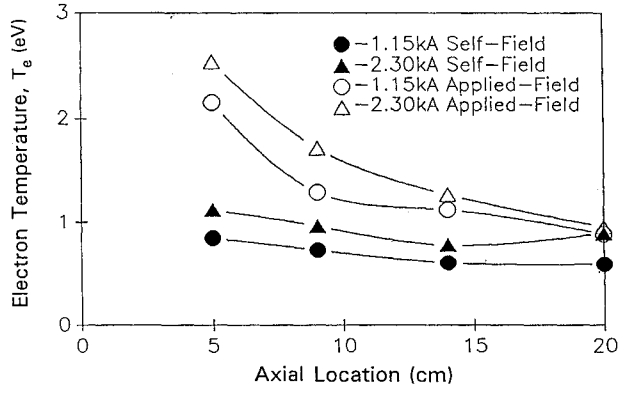

Fig. 9 Axial variation of *Te* from langmuir probe data.

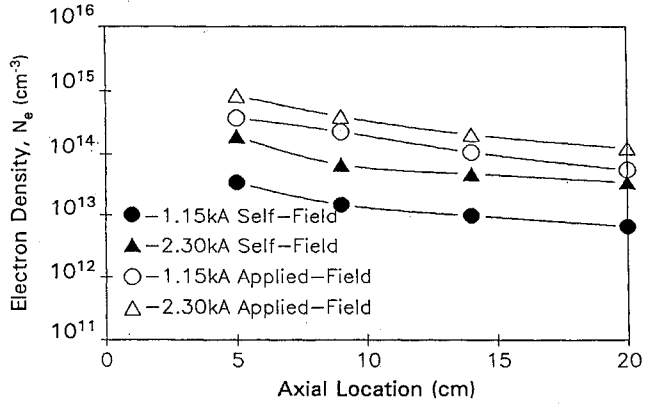

Fig. 10 Axial variation of *Ne* from langmuir probe data.

Table 2 One-fourth scale thruster performance parameters

	Electrothermal thrust, N	Electromagnetic thrust, N	Total thrust, N	Flow velocity, m/s
		1.15-kA Case		
Self-Field				
Theoretical	0.80	0.31	1.11	8,300
Experimental	—	—	1.17 (P[a])	6,950 (L, P[b])
Applied-Field				
Theoretical	0.80	0.31	1.11	8,300
Experimental	—	—	1.82 (P)	11,080 (L, P)
		2.30-kA Case		
Self-Field				
Theoretical	0.90	1.25	2.15	16,100
Experimental	—	—	3.02 (P)	10,030 (L, P)
Applied-Field				
Theoretical	0.90	1.25	2.15	16,100
Experimental	—	—	5.02 (P)	11,100 (L, P)

[a]P: Det. using impact pressure. [b]L, P: Det. using N_e, T_e from Langmuir, nmu[2] from pressure.

ment in the plasma which was not related to a voltage increase in the discharge chamber.

Thrust and Exhaust Velocity Evaluations

Using electrical discharge parameters, theoretical values of electrothermal and electromagnetic thrust for the device were evaluated. For the self-field discharge, electrothermal thrust was estimated using a limiting value which assumes complete expansion, $T_{eth} = \dot{m}(2C_pT_0)^{1/2}$; while the electromagnetic component was calculated using

$$T_{em} = (\mu_0 I^2/4\pi)[\ln(R_A/R_C) + \tfrac{3}{4}] \quad (9)$$

Since the applied magnetic fields did not enter the discharge chamber and the power input with applied field nozzles did not change, these values will also be used for comparison with applied nozzle experiments.

Experimental values of thrust were evaluated by integrating impact pressure over a cross section of jet at an axial location where pressure signals reached their maximum. Values of velocity were evaluated from input pressure data, using N_e and T_e from langmuir probes. Using theoretical total thrust values, an effective velocity was evaluated from $U_{eff} = T/\dot{m}$. A compilation of plasma acceleration parameter is presented in Table 2. It can be concluded that for the self-field discharge, thrust increased with increased power. However, in both cases, the exhaust velocities derived from experiment were lower than the theoretical estimates by factors of 0.85 and 0.62. With the addition of applied magnetic nozzles, the thrust increased for both power levels by a factor of 1.6. The exhaust velocity derived from experiment increased by factors of 1.6 (1.15 kA) and 1.1 (2.3 kA) with the applied magnetic nozzles. These values of exhaust velocity derived from experiment were lower and higher than the theoretical estimates, so the details of plasma expansion in the two cases appear to be different.

Conclusions

The influence of applied magnetic nozzles on the performance of a low-power MPD thruster was examined in the unique condition where the magnetic field did not penetrate the discharge chamber or alter the power delivered to the thruster. The applied magnetic nozzles resulted in increased plasma density and temperature in the exhaust flow outside the discharge chamber. Thrust and exhaust velocities derived from experimental data were found to increase by factors of 1.6, due to the applied magnetic nozzles.

References

[1]Sovey, J. S., and Mantenieks, M. A., "Performance and Lifetime Assessment of MPD Arc Thruster Technology," AIAA Paper 88-3211, July 1988.

[2]Seikel, G. R., York, T. M., and Condit, W. C., "Applied-Field Magnetoplasmadynamic Thrusters for Orbit-Raising Missions," *Orbit-Raising and Maneuvering Propulsion: Research and Needs*, edited by L. H. Caveny, Vol. 89, Progress in Astronautics and Aeronautics, AIAA, New York, 1984, pp. 260–286.

[3]Connolly, D. J., Bishop, A. R., and Seikel, G. R., "Tests of Permanent Magnet and Superconducting Magnet MPD Thrusters," AIAA Paper 71-196, June 1971.

[4]Michels, C. J., and York, T. M., "Pressure Measurements in the Exhaust of a Pulsed Megawatt MPD Arc Thruster," AIAA Paper 71-196, Jan. 1971.

[5]Michels, C. J., and York, T. M., "Exhaust Flow and Propulsion Characteristics of a Pulsed MPD Arc Thruster," AIAA Paper 72-500, April 1972.

[6]Fradkin, D. B., Blackstock, A. W., Roehling, D. J., Stratton, T. F., Williams, M., and Liewer, K. W., "Experiments Using a 25-kW Hollow Cathode Lithium Vapor MPD Arcjet," *AIAA Journal*, Vol. 8, May 1970, pp. 886–894.

[7]Kimura, I., and Arakawa, Y., "Effect of Applied Magnetic Fields on Physical Processes in an MPD Arcjet," *AIAA Journal*, Vol. 15, May 1977, pp. 721–724.

[8]Tahara, H., Kagaya, Y., and Yoshikawa, T., "Quasi-Steady MPD Arcjets with Applied Magnetic Fields," AIAA Paper 85-2001, Oct. 1985.

[9]Arakawa, Y., and Sasoh, A., "Steady-State Permanent Magnet Magnetoplasmadynamic Thruster," *Journal of Propulsion and Power*, Vol. 3, No. 3, 1989, pp. 301–304.

[10]Kuriki, K., and Okada, O., "Experimental Study of Plasma Flow in a Magnetic Nozzle," *Physics of Fluids*, Vol. 13, Sept. 1970, pp. 2262–2268.

[11]Mantenieks, M. A., Sovey, J. S., Myers, R. M., Haag, T. W., and Raitano, P., "Performance of a 100 KW Class Applied Field MPD Thruster," AIAA Paper 89-2710, July 1989.

[12]King, D. Q., Smith, W. W., Jahn, R. G., and Clark, K. E., "Effect of Thrust Chamber Configuration on MPD Arcjet Performance," AIAA Paper 79-2051, Oct. 1979.

[13]Mead, F. M., and Jahn, R. G., "Scaling of MPD Thrusters," AIAA Paper 79-2075, Oct. 1979.

[14]Kaplan, D. I., "Performance Characteristics of Geometrically Scaled MPD Thrusters," M.S. Thesis, Princeton Univ., Princeton, NJ, Feb. 1982.

[15]Gilland, T. H., Kelly, A. J., and Jahn, R. G., "MPD Thruster Scaling," AIAA Paper 87-0997, May 1987.

[16]Minns, F. M., III, *Engineer's Mini-Notebook: Op-Amp Circuits*, Archer Pub., Ft. Worth, TX, 1985.

[17]York, T. M., "Stress Dynamics in High Speed Piezoelectric Pressure Probes," *Review of Scientific Instruments*, Vol. 41, April 1970, pp. 519–521.

[18]Kenney, T. M. P., "Measurements of Pressure Profiles in the Exhaust Plume of a Magnetoplasmadynamic Thruster," M.S. Thesis, Pennsylvania State Univ., University Park, PA, Dec. 1987.

[19]Jahn, R. G., *Physics of Electric Propulsion*, McGraw-Hill, New York, 1969.

[20]Chen, F. F., *Plasma Physics and Controlled Fusion*, Plenum Press, New York, 1984.

[21]Pai, S.-I., *Magnetogasdynamics and Plasma Dynamics*, Prentice-Hall, Englewood Cliffs, NJ, 1962.

[22]Yoshikawa, T., Kagaya, Y., and Tahara, H., "Thrust Measurement of a Quasi-Steady MPD Arcjet," AIAA Paper 85-2003, Oct. 1985.

[23]York, T. M., Mikellides, P., and Jacoby, B. A., "Plasma Flow Processes Within Magnetic Nozzle Configurations," *Journal of Propulsion and Power*, Vol. 8, No. 5, 1992, pp. 1023–1030.

[24]Chung, P. M., Talbot, L., and Touryan, K. J., *Electric Probes In Stationary and Flowing Plasma: Theory and Application*, Springer-Verlag, New York, 1975.